Environmental Science and Pollution Research (2019) 26:4180–4191
https://doi.org/10.1007/s11356-018-2314-6

ADVANCED OXIDATION TECHNOLOGIES: STATE-OF-THE-ART IN IBERO-AMERICAN COUNTRIES

Phosphorous-doped TiO_2 nanoparticles: synthesis, characterization, and visible photocatalytic evaluation on sulfamethazine degradation

Sandra Yadira Mendiola-Alvarez[1] · Ma. Aracely Hernández-Ramírez[1] · Jorge Luis Guzmán-Mar[1] · Lorena Leticia Garza-Tovar[1] · Laura Hinojosa-Reyes[1]

Received: 1 February 2018 / Accepted: 13 May 2018 / Published online: 24 May 2018

Abstract

Mesoporous phosphorous-doped TiO_2 (TP) with different wt% of P (0.5, 1.0, and 1.5) was synthetized by microwave-assisted sol–gel method. The obtained materials were characterized by XRD with cell parameters refinement approach, Raman, BET-specific surface area analysis, SEM, ICP-OES, UV–Vis with diffuse reflectance, photoluminescence, FTIR, and XPS. The photocatalytic activity under visible light was evaluated on the degradation of sulfamethazine (SMTZ) at pH 8. The characterization of the phosphorous materials (TP) showed that incorporation of P in the lattice of TiO_2 stabilizes the anatase crystalline phase, even increasing the annealing temperature. The mesoporous P-doped materials showed higher surface area and lower average crystallite size, band gap, and particle size; besides, more intense bands attributed to O–H bond were observed by FTIR analysis compared with bare TiO_2. The P was substitutionally incorporated in the TiO_2 lattice network as P^{5+} replacing Ti^{4+} to form Ti–O–P bonds and additionally present as PO_4^{3-} on the TiO_2 surface. All these characteristics explain the observed superior photocatalytic activity on degradation (100%) and mineralization (32%) of SMTZ under visible radiation by TP catalysts, especially for P-doped TiO_2 1.0 wt% calcined at 450 °C (TP1.0-450). Ammonium, nitrate, and sulfate ions released during the photocatalytic degradation were quantified by ion chromatography; the nitrogen and sulfur mass balance evidenced the partial mineralization of this recalcitrant molecule.

Keywords Phosphorous-doped TiO_2 · Mesoporous material · Heterogeneous photocatalysis · Visible light · Sulfamethazine · Microwave-assisted sol–gel method

Introduction

The extensive use of veterinary pharmaceuticals to treat infections and improve growth and feed efficiency has raised concern due not only to the development of resistant bacteria strains that represent a health risk to humans and animals but also in other environmental impairments (Martínez 2009).

The sulfamethazine (4-amino-*N*-(4,6-dimethylpyrimidine-2-yl)benzenesulfonamide, SMTZ) is the most widely used antimicrobial agent in veterinary medicine to treat infections by gram-positive and gram-negative bacteria. This compound has been detected in drinking water wells (0.22 μg/L) (Batt et al. 2006) and river waters (2.48 μg/L) (García et al. 2010). Conventional water and wastewater processes are unable to efficiently remove recalcitrant pollutants as SMTZ (Ben et al. 2014); thus, it is necessary to evaluate alternative treatment technologies as heterogeneous photocatalysis for the degradation of this toxic and emerging organic pollutant. This process consists of the absorption of radiant energy (UV or visible) by a light-sensitive broadband semiconductor. When semiconductor catalyst is illuminated with photons energy equal or greater than band gap energy of catalyst ($h\upsilon \geq Eg$), they are absorbed, and electron–hole pairs are created within the bulk. If charge separation is maintained, the electron and hole may migrate to the catalyst surface where they participate in redox

Responsible editor: Suresh Pillai

Electronic supplementary material The online version of this article (https://doi.org/10.1007/s11356-018-2314-6) contains supplementary material, which is available to authorized users.

✉ Laura Hinojosa-Reyes
laura.hinojosary@uanl.edu.mx

[1] Facultad de Ciencias Químicas, Cd. Universitaria, Universidad Autónoma de Nuevo León, UANL, C.P. 66455 San Nicolás de los Garza, N. L., México

reactions with sorbed species (Bahadur et al. 2013). TiO_2 is one of the most studied photocatalysts due to its abundance, low cost, low toxicity, superior photo-stability, and high intrinsic catalytic activity under UV illumination (Miranda et al. 2014).

However, the photoconversion efficiency of TiO_2 is limited to less than 2.2% under solar illumination owing to its large band gap energy (3.2 eV for anatase phase) that is generally considered to be more active than rutile phase (Devi and Kavitha 2013). For this reason, doping with non-metals as phosphorus into TiO_2 has been proved to be an excellent strategy to extend TiO_2 band gap from the UV to the visible light region through modifying its electronic band structure by the creation of local states inside the band (Gopal et al. 2012). The photocatalytic enhancement of P-doping TiO_2 has been attributed to the narrowed band gap, the reduction in the electron–hole pair recombination rate (Mohamed and Aazam 2013), and the increased surface area. The other benefit reported for P-doping TiO_2 is that the surface-bound phosphate increases the thermal stability of the TiO_2 anatase phase, retarding the transition to rutile phase (Chen et al. 2011; Xia et al. 2014) and maintaining mesoporous structure (Yu et al. 2003) after annealing at high temperature. Improved photocatalytic activity has been described for TiO_2 in anatase crystalline phase than rutile and amorphous TiO_2 (Yu et al. 2009). Previous studies have been reported that the doped P atoms occurred in two chemical forms in the TiO_2 structure, as superficial phosphate (PO_4^{3-}) in a tetrahedral environment (Mohamed and Aazam 2013; Niu et al. 2014), whereas some other works described that P is incorporated as P^{5+} oxidation state substituted the lattice Ti^{4+} forming Ti–O–P bonds in an environment of a coordination number 6 (Zhu et al. 2008; Ma et al. 2014). A positive role in enhancing the photocatalytic activity has been described for P incorporated in the TiO_2 lattice in a substitutional way (Lv et al. 2009; Guo et al. 2010; Kuo et al. 2015). The P-doping TiO_2 has been synthesized by different methods such as modification of TiO_2 Degussa P25 with H_3PO_4 (Kuo et al. 2015), one-step ball milling process (Ansari and Cho 2016), microwave hydrothermal method (Niu et al. 2014), and sol–gel approach (Gopal et al. 2012; Mohamed and Aazam 2013; Xia et al. 2014). Among the different methods, the sol–gel process has become the most widely used method for the synthesis of semiconductor photocatalysts. This procedure allows the incorporation of dopant ions at the molecular level. Other advantages include the production of high-purity nanosize particles and the homogeneity of the products (Cervantes Rojas 2012). This process can additionally be assisted by microwave in order to obtain materials with greater photocatalytic activity because microwave energy provides rapid heating, higher reaction speed and selectivity, low reaction temperature, short reaction time, homogeneous thermal transference, purity of phases, fast crystallinity due to the fact that it promotes nucleation of the crystals in short time, smaller particle size, and higher reaction yields (Tongon et al. 2014). The enhancement in photocatalytic activity was observed in P-doped TiO_2 during degradation of different contaminants like methylene blue under visible radiation (Niu et al. 2014), methyl orange under UV radiation (Xia et al. 2014), and bisphenol A using solar radiation (Kuo et al. 2015). Thus, in the present work, a simple microwave-assisted sol–gel method for the synthesis of mesoporous P-doped TiO_2 catalyst with high specific surface area is reported. We investigated in detail how the increasing amount of P and the annealing temperature influenced the structural and optical properties of P-doped TiO_2, and how these properties play a vital role in the photocatalytic activity toward photooxidation of SMTZ in aqueous medium under visible radiation. The SMTZ degradation kinetics and evolution of ions (NH_4^+, NO_3^-, and SO_4^{2-}) during photocatalytic reactions were also evaluated.

Experimental procedure

Reagents

All reagents were analytical grade quality. Titanium (IV) isopropoxide (97%) and phosphoric acid (99%) were obtained from Sigma-Aldrich (St. Louis, MO, USA) and used as precursors for the synthesis of P-doped materials. Titanium dioxide P25 with a composition of 80% anatase and 20% rutile, 50 ± 1.0 m^2/g of specific surface area, and approximately 20 nm crystallite size with mesoporous structure was purchased from Degussa Chemicals (Hanau, Germany). This semiconductor was used as a reference catalytic material in photocatalytic processes for comparative purposes due to its extended application in this field. A stock solution of 100 mg/L SMTZ was prepared with double-distilled water using sodium salt sulfamethazine (98%, Sigma-Aldrich) and stored at 4 °C in dark glass bottles. Ammonium acetate (98%) and methanol HPLC grade (99.9%) used to prepare HPLC mobile phase were from Sigma-Aldrich. Sodium carbonate (99.9%), sodium bicarbonate (99.7%), and 0.1 M methanesulfonic acid used for ionic chromatography analysis were purchased from Sigma-Aldrich.

Catalyst synthesis

The P-doped TiO_2 materials were synthesized by microwave-assisted sol–gel method with a molar ratio of 1:8:3 (titanium/water/isopropanol). A mixture of isopropanol and double-distilled water were placed under magnetic stirring for 30 min in a three-necked Pyrex flask and then adjusted the pH of the solution to 3.0 with acetic acid. The corresponding quantity of phosphoric acid to obtain 0.5, 1.0 and 1.5 wt% was mixed with water and isopropanol in a Pyrex beaker. At the

time, the phosphoric acid/water/isopropanol solution mixture and the titanium(IV) isopropoxide were added drop by drop at the flask with isopropanol/water solution. The mixture was kept continuously stirred at room temperature for 2 h to obtain transparent sol that was transferred into a 75-mL capacity Teflon vessel and irradiated inside a microwave system (MARS 6, CEM) during 60 min at 150 °C. The white colored powders were collected, filtered, and washed with distilled water and dried at 80 °C for 20 h. Afterwards, samples were calcined at 450, 550, and 650 °C for 4 h (2 °C/min temperature rate) in a muffle furnace (Barnstead Thermolyne). For comparison, bare TiO_2 was prepared by the same methodology without adding phosphoric acid. The prepared materials were denoted as Ty for undoped TiO_2, and TP*xy* for doped materials, where *x* refers wt% of P incorporated and *y* denotes calcination temperature.

Characterization

The phase structure of the synthesized nanocatalysts was examined using X-ray diffraction analyzer (Bruker AXS Model D2 Phaser Instrument) and database JCPDS-ICDD reference standards. This analysis was performed in 2θ range from 15° to 90° and scanning rate of 0.02°/0.5 s using monochromatic detector with Cu Kα radiation (1.5418 Å). KCl was used as internal standard in the ratio catalyst/standard 10/1 to obtain XRD measurements for cell parameters refinement. The average crystallite size (Eq. 1) was estimated by measuring the full width at half maximum of the most intense diffraction peak using the Debye–Scherrer equation:

$$D = \frac{k\lambda}{\beta\cos\theta} \quad (1)$$

where D is the average crystallite size; k is the Scherrer constant, which is usually taken as 0.9, λ is the wavelength of radiation used; β is the angular width of the diffraction peak at the half maximum (FWHM) on the 2θ scale; and θ is the Bragg angle. The refined unit cell parameters were achieved for the analysis of the pure and phosphorous-doped TiO_2 samples using the UnitCell software for indexing. Raman spectra were recorded in a wavelength range from 100 to 1000/cm with a Raman equipment (NRS-5100, JASCO) using a 785-nm power diode laser (excitation with 10.8 mW) with a charge coupled device (CCD) detector. The BET surface area, pore volume, and pore size distributions were determined by using a micromeritics (TriStar II 3020 Micromeritics Instrument Corporation) nitrogen adsorption/desorption apparatus. The particle morphology of samples was analyzed by scanning electron microscopy (SEM) using a Hitachi S-3400N microscope operated at 15 kV. The incorporated P (wt%) in the catalysts was determined by Inductively Coupled Plasma Optical Emission Spectroscopy (ICP-OES) in a PerkinElmer Optima 4300DV; the detection wavelength was 214.914 nm. Catalyst materials were previously digested with HF/HNO_3/HCl (1:3:1) at 180 °C for 20 min in a MARS 6 CEM microwave oven. The light absorption properties of the semiconductors were analyzed by UV–Vis diffuse reflectance spectra (DRS) using UV–Vis spectrophotometer (Evolution 300 PC, Nicolet) equipped with an integrating sphere assembly. Diffuse reflectance spectra were measured from 200 to 800 nm using barium sulfate ($BaSO_4$) as the reflectance reference standard. The photoluminescence (PL) spectra were acquired at room temperature in Horiba Scientific model FL-1000 series 4637-134 using excitation wavelength of 345 nm. The luminescence intensity was measured over the wavelength range 380 to 660 nm. KBr-pressed pellets were used to characterize the P-doped TiO_2 materials by FTIR. Spectra were recorded from 4000 to 400/cm on a Vertex 70 FTIR spectrometer (Bruker Optics Inc., Billerica, MA) that was equipped with a liquid N_2(I)-cooled HgCdTe detector (InfraRed Associates Inc.). The spectral resolution was 4/cm and 64 scans were collected per spectrum. The KBr background spectrum was subtracted from the measured spectrum of the catalysts to provide the FTIR characterization data. X-ray photoelectron spectroscopy (XPS) measurements were recorded using an X-ray photoelectron spectrometer (PHI 5000 Versa Probe II) with an Al Kα radiation source.

Photocatalytic evaluation

The photocatalytic activity was tested on the degradation of SMTZ under visible radiation with a Phillips Hg lamp (450–600 nm, 1000 W/m^2). The degradation experiment was performed in a batch reactor (Pyrex beaker) containing 450 mL of aqueous 10 mg/L SMTZ solution at pH 8.0 and a fixed catalyst loading of 1 g/L. The aqueous solution was previously adjusted at the desired pH with 0.1 M NH_4OH, using a pH/ISE meter Orion Star A111 (Thermo Scientific). The suspension was stirred in the dark for 1 h before irradiation to ensure the adsorption–desorption equilibrium. The lamp was positioned 10.0 cm above the photo-reactor, and the experiments were performed at room temperature (25 ± 2 °C). The reaction rate was followed by taking aliquots at desired time intervals and then filtered with a 0.45-μm Regenerated Cellulose PHENEX syringe filter. Monitoring of SMTZ degradation was followed injecting 25 μL of sample by reversed phase high-performance liquid chromatography (HPLC, PerkinElmer) with UV–Vis detection (264 nm) using a Luna C8 100 × 4.6 mm, 3-μm column (Phenomenex). The mobile phase was 20 mM ammonium acetate/methanol 65:35 (*v*/*v*) at a flow rate of 1 mL/min; these chromatographic conditions were adapted from a previous study (García-Galán et al. 2010). The total organic carbon (TOC) concentration during

the degradation process was determined in the aqueous solution using a TOC-V CSH Shimadzu Analyzer. Nitrate, sulfate, and ammonium ions were analyzed by ionic chromatography (Dionex ICS-1100, Thermo Scientific). For the determination of the anions, the mobile phase used was 4.5 mM Na_2CO_3/0.8 mM $NaHCO_3$ at a flow rate of 1.5 mL/min with a Dionex Ion Pac® AS23 column (250 × 4 mm, Thermo Scientific). The amount of ammonium ion was measured using a Dionex IonPac® CS12A (4 × 250 mm, Thermo Scientific) column with a 20 mM methanesulfonic acid as mobile phase at a flow rate of 1 mL/min.

Results and discussion

Characterization of catalysts

Figure 1a represents the XRD patterns of P-doped TiO_2 catalysts calcined at 450 °C. The patterns showed that all the samples present the anatase crystalline phase (JCPDS 21-1272). The XRD patterns did not exhibit P-related peak in P-TiO_2 samples due to P ions that were uniformly dispersed within the anatase crystalline structure or because the doping amount was too low. These results demonstrated that the addition of P had no influence on the crystalline phase but influenced the TiO_2 crystallization process by modifying the crystallite size. With the increase of P-doping amount, broad and weak peaks were observed compared T-450 sample, which affected in the lower crystallite size (Mohamed and Aazam 2013; Niu et al. 2014). The crystallite size of materials was calculated by Scherrer's equation (Table 1). It can be seen that the average crystallite size of P-doped TiO_2 was smaller than that of undoped TiO_2. This decrease in crystallite size upon doping amount can be ascribed to the distribution of P dopant in TiO_2 lattice. Moreover, the peak corresponding to the plane (1 0 1) showed in Fig. 1b exhibits a slight shift from 25.36° in T-450 to 25.34° for doped materials with 0.5 and 1.0% of P and to 25.28° for TP1.5-450 sample. The shift of the plane (1 0 1) can be attributed to a perturbation in the anatase crystalline phase for the incorporation of P ion (Hsuan-Fu 2007). The ionic radius of P^{5+}, O^{2-} and Ti^{4+} are 0.35, 1.32, and 0.68 Å, respectively (Kuo et al. 2015). Thus, the P^{5+} was incorporated in the TiO_2 crystal lattice originating structural defects of the TiO_2 network by partly replacing Ti^{4+} (Zhang et al. 2009). Several authors (Zhu et al. 2008; Lv et al. 2009; Guo et al. 2010; Kuo et al. 2015) observed that doping TiO_2 with P increase the thermal stability of anatase phase. The transformation of anatase to rutile phase in undoped TiO_2 was described between 500 and 700 °C annealing temperature (Körösi et al. 2007). Thus, in this work, TP1.0 was annealed at three different temperatures (450, 550, and 650 °C) to evaluate the thermal stability of anatase phase for a P-doped TiO_2. The XRD results (supplementary material Fig. S1) shows that only anatase crystalline phase for all materials was present, suggesting that the transition from anatase to rutile phase was retarded by doping with phosphorous according to previous reports (Chen et al. 2011). The average crystallite size of P-doped TiO_2 materials increased with the increment of

Table 1 Average crystallite size and cell parameters for P-doped and undoped catalyst calcined at 450 °C

Catalyst	Crystallite size (nm)[a]	Cell parameters[b]		
		$a = b$ (Å)	c (Å)	Volume (Å^3)
T-450	16.54	3.788(1)	9.514(1)	136.577(9)
TP0.5-450	6.83	3.794(6)	9.485(2)	136.578(9)
TP1.0-450	6.43	3.799(3)	9.516(8)	137.388(1)
TP1.5-450	6.10	3.807(0)	9.506(1)	137.778(8)

Numbers in the parenthesis represents standard deviation

[a] Scherrers equation

[b] Indexing method

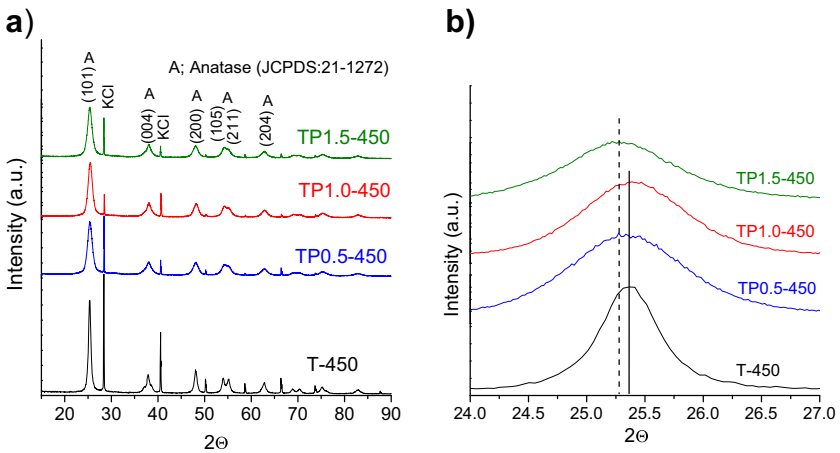

Fig. 1 **a** XRD patterns of T-450, TP0.5-450, TP1.0-450, and TP1.50-450 using KCl as internal standard and **b** (1 0 1) XRD peak positions of the anatase for the catalyst obtained with different percentages of P

annealing temperature with values between 6.43, 7.46, and 9.83 nm for TP1.0-450, TP1.0-550, and TP1.0-650, respectively, and the increase of the annealing temperature delayed the crystallization process of anatase (Körösi et al. 2007; Zhu et al. 2008).

With XRD patterns and the cell parameter refinement method that were determined, the cell parameters of the catalysts were calcinated at 450 °C. The parameters obtained were $a = b$ and c, because the anatase crystalline phase has a body centered tetragonal structure and belongs to the space group 14I/amd.

The cell parameters a, b, and volume determined by internal standard refinement method of TP materials increased compared to those values of bare TiO_2. Although the ionic radius of P (0.35 Å) is smaller than that of Ti (0.68 Å), the arrangement of the dopant in the anatase crystal lattice produced an increase of the cell parameters $a = b$ and volume. The same tendency was reported by different authors (Hsuan-Fu 2007; Li et al. 2009; Elghniji et al. 2012; Xia et al. 2014; Sotelo-Vazquez et al. 2015). In accordance with (Li et al. 2009), the expansion of unit cell might be attributed to the introduction of oxygen (2^-) into the TiO_2 lattice for the electrostatic balance of P^{5+}. These observations confirmed that P incorporation into TiO_2 lattice in a substitutional doping way modifies the tetragonal crystal structure of anatase TiO_2.

As shown in Fig. S2 (supplementary material), Raman measurements showed peaks at 197 Eg, 395 B_{1g}, 516 A_{1g} + B_{1g}, and 638 Eg, confirming only the anatase phase for all materials. No peaks corresponding to P–O (1035, 1047, and 1073/cm) were exhibited (Li et al. 2009). It has been described that decrease in particle size observed due to the incorporation of P in TiO_2 lattice in P-doped TiO_2 would decrease the Raman intensity peaks (Lv et al. 2009).

The surface area, pore volume, and pore size of all samples are summarized in Table 2. The BET surface area of TiO_2 was 73.95 m^2/g and increased up to 158.85, 173.81, and 188.59 m^2/g with 0.5, 1.0, and 1.5 wt% P doping, respectively. Yu et al. (2003) explained that doping with P causes stability of the framework and avoids the collapse of the mesoporous walls of TiO_2, which occur during the calcination process due to the rapid reactions between uncondensed Ti–OH. Larger surface area can also be attributed to the suppression of TiO_2 crystal growth by P (Mohamed and Aazam 2013). Comparable results were obtained by Gopal et al. (2012) that prepared TP 1.3 wt% by sol–gel method and calcined at 500 °C with surface area of 174.42 m^2/g. Furthermore, the mesoporous structure of TiO_2 and P-doped TiO_2 catalysts was confirmed by the adsorption–desorption isotherms (Fig. S3), classified according to the IUPAC as type IV and hysteresis loop type H1, which are related with agglomerated and spherical particles (Ermokhina et al. 2013). Similarly, BJH adsorption pore volume increased with the increase in P-doping amount while pore diameter decreased with P-doping up to 1.0 wt% of P content. Thus, the increase in pore volume with reduced pore diameter was possibly due to the controlled crystal growth in the P-doped TiO_2 samples (Gopal et al. 2012). Mesoporous materials are related with large surface areas, which are an important advantage in photocatalysis since those materials present more active sites to carry out photocatalytic process (Yu et al. 2003). All these results are consistent with previous reports (Li et al. 2009; Elghniji et al. 2012; Gopal et al. 2012). On the other hand, related to the effect of calcination temperature, some authors (Hsuan-Fu 2007; Körösi et al. 2007; Li et al. 2009; Chen et al. 2011; Iwase et al. 2013a, b) have described lower surface area and higher crystallite size when increasing the annealing temperature for P-doped TiO_2 materials. In this work, surface area for samples calcined at different temperatures was not evaluated; however, crystallite size for these materials decreased as reported in XRD section. Thus, we could infer lower specific surface area values for samples calcined at higher temperatures than 450 °C.

The SEM micrographs of samples are illustrated in Fig. 2. According to SEM images, spherical morphology was formed, and particles were agglomerated. Particle size decreased as phosphorous doping concentrations increased from 0.5 to 1.5 wt%. The average particle sizes were 23.9, 16.1, 13.8, and 12.3 nm for T-450, TP0.5-450, TP1.0-

Table 2 Physiochemical characterization of T-450, TP0.5-450, TP1.0-450, and TP1.50-450

Catalyst	Eg (eV)[a]	Theoretical P content (wt%)	Incorporated P content (wt%)[b]	Surface area (m^2/g)[c]	Total pore volume (cm^3/g)[d]	Average pore size (nm)[d]
T-450	3.08	–	–	73.90	0.14	6.07
TP0.5-450	3.04	0.5	0.45 ± 0.03	158.85	0.29	6.78
TP1.0-450	2.99	1.0	0.81 ± 0.04	173.80	0.32	6.83
TP1.5-450	2.96	1.5	1.33 ± 0.01	188.59	0.37	7.69

[a] UV–Vis with DRS

[b] ICP-OES

[c] BET

[d] BJH

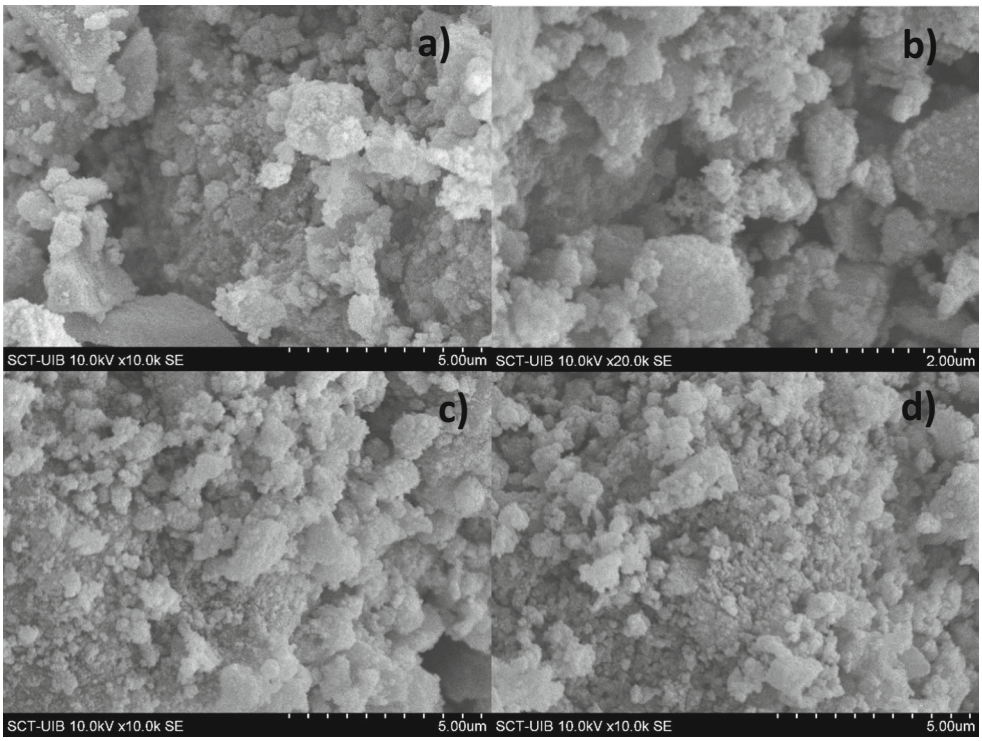

Fig. 2 SEM images of nanoparticles. **a** T-450. **b** TP0.5-450. **c** TP1.0-450. And **d** TP1.50-450

450, and TP1.50-450, respectively. The, P content was determined in the P-doped materials by ICP-OES technique. The results are shown in Table 2. The amount of P incorporated was from 81 to 90% with respect to theoretical values, and the small differences between theoretical and incorporated P could be attributed to errors during the catalyst synthesis, digestion, and ICP-OES analysis.

The band gap energy (Eg) values were calculated from the plot of the Kubelka–Munk function versus energy (Fig. S4) and are shown in Table 2. The Eg values for undoped and P-doped TiO_2 ranged from 3.08 to 2.96 eV. A small decrease in the band gap with increasing phosphorous content in TiO_2 catalysts was observed. The reduction of the Eg was closely related to the increasing of P percentage. Thus, the lowering in the Eg values of P-doped TiO_2 materials has been described (Shi et al. 2006; Li et al. 2009) and indicated that these P-doped materials could be activated under irradiation in the visible region (Kesong et al. 2007). Based on functional density theory calculations, the electronic structure of P-doped anatase TiO_2 was studied and found that the band gap narrowing was due to the substitution of Ti^{4+} by P^{5+}. Likewise (Shi et al. 2006) attributed, the red shift in the band gap might be due to the P incorporation on TiO_2 lattice. As can be seen in Fig. S4, none additional band was observed in the visible region of the spectra of the white P-doped TiO_2 powders calcined at 450 °C.

Photoluminescence (PL) emission spectra (Fig. 3) were used to investigate the ability to stabilize the charge and reduce the recombination of the e^-/h^+ pairs in the semiconductor. Overall, high intensity emission on PL reflects quick electron/hole recombination rate, while low-intensity emission implies slower charge recombination rate (Ansari and Cho 2016). The reduced PL intensity for P-doped TiO_2 catalyst was due to the P incorporated into TiO_2, hindering electron–hole pair recombination rate on the P-doped TiO_2 surface. Thus, this semiconductor material could present greater photocatalytic activity (Mohamed and Aazam 2013). For both catalysts, four exitonic signals were observed in 398, 471,

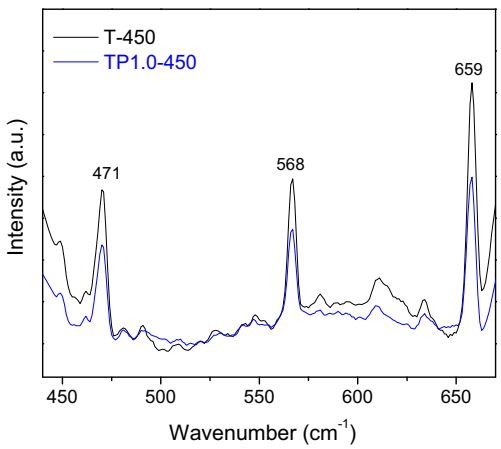

Fig. 3 Photoluminescence spectra of T-450 and TP1.0-450

568, and 659 nm corresponding to the UV, blue, yellow, and orange regions of the visible spectrum, respectively. The emission in the UV at 398 nm generally exhibits the transition of free electrons from the low level of oxygen vacancies to the TiO_2 valence band. While the peaks in the visible region (471, 568, and 659 nm) were attributed to oxygen vacancies with two and one trapped electron to the TiO_2 valance band (Guo et al. 2013). The recombination of photogenerated carriers via transition from the oxygen vacancies to TiO_2 valance band was suppressed efficiently upon doping with P ions.

The FTIR spectra of the materials with different amounts of P are shown in Fig. 4a. The broadbands at 3240 and 1640/cm for undoped and doped TiO_2 could be attributed to the –OH stretching and bending vibrations of chemical adsorbed water and hydroxyl groups (Lin et al. 2007). When the content of P increases, these bands became broader and stronger than that for the undoped TiO_2. According to Li et al. (2009), the doping with P was responsible for high adsorption capacity of the TiO_2 powders due to their large surface area. Three additional broad absorption bands (Fig. 4b) at 1040, 1095, and 1125 cm^{-1} were observed in the doped materials, suggesting the chemical environment of the P in the TiO_2. These bands are attributed to P–O vibration (Xia et al. 2014). The broad peak at 1095 cm^{-1} is characteristic ν3 vibration of the phosphate ions coordinated with TiO_2. The band at 1125 cm^{-1} is related with ν2 vibration of the phosphate in a bidentate state (associating at surface), and the shoulder peak at 1040 cm^{-1} belongs to Ti–O–P framework vibrations (Elghniji et al. 2012). That means that P species possibly would exist in the surface (as bidentate phosphate) and in the lattice forming Ti–O–P bonds (Körösi et al. 2007). The broad adsorption peak present at 800 cm^{-1} for all materials is assigned to Ti–O–Ti vibration if Ti is in octahedral environment (Yu et al. 2003).

The chemical composition of the catalysts was investigated by XPS. The Fig. 5a shows the binding energy of the TP1.0-450 corresponding to O 1s, Ti 2p, and P 2p. Figure 5b shows the binding energy of the Ti 2p for T-450 and TP1.0-450. The peaks of the binding energies in the TiO_2 catalyst were observed at 458.1 and 463.9 eV for Ti 2p 3/2 and Ti 2p 1/2, respectively. The signals were slightly shifted to higher binding energies for P-doped TiO_2 (464.2 and 458.5 eV). The shifts to higher binding energies with respect to TiO_2 were due to the substitution of Ti^{4+} with more electronegative species P^{5+}, pulling the electrons in the Ti-O bond away from the Ti (Mohamed and Aazam 2013). The spectra region corresponding to O 1s is shown in Fig. 5c for samples T-450 and TP1.0-450. The peak for T-450 was 528.6 eV, while for sample TP1.0-450, it shifted to a higher value (529.7 eV) and in agreement with the different electronegativity values of phosphorus, titanium, and oxygen. The deconvolution of the peak O 1s of TP1.0-450 sample (see Fig. 5d) shows that two signals at binding energies of 529.49 and 530.57 eV belonged to Ti–O and P–O bonds, respectively; these results support the theory that P^{5+} replaced Ti^{4+} by forming Ti–O–P bonds (Ansari and Cho 2016).

Phosphorus in the catalyst showed a characteristic peak in 133.7 eV corresponding to P 2p. This signal was attributed to the P^{5+} (Gopal et al. 2012). Based on the ionic radius of P^{5+} (0.35 Å) and Ti^{4+} (0.68 Å) (Li et al. 2009), the P^{5+} could replace the Ti^{4+} in the crystal lattice. The replacement of Ti^{4+} by P^{5+} induces charge imbalance by the formation of Ti–O–P bonds (Gopal et al. 2012) that can help to reduce the recombination of the photogenerated e^-/h^+ pairs. Additionally, it is important to note that the signal at 128.6 eV attributed to Ti–P bond when the P that replaces the O in the crystal lattice was not observed (Guo et al. 2010). These results are also consistent with FTIR results.

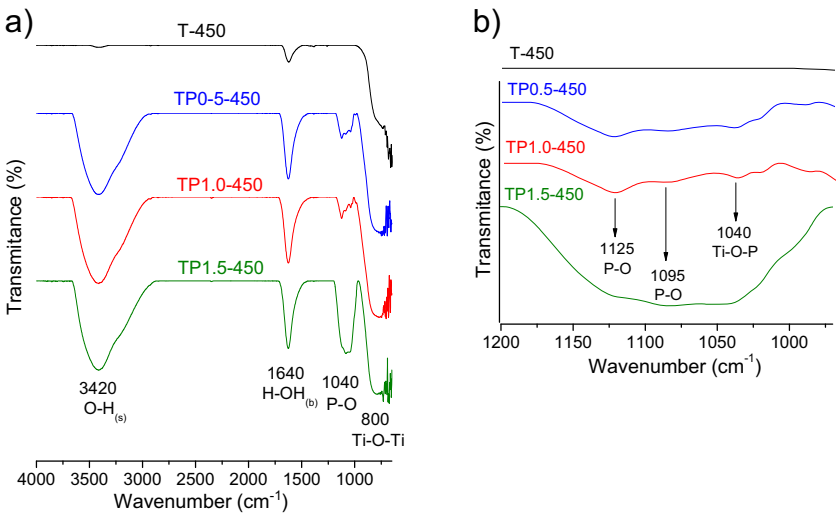

Fig. 4 **a** FTIR spectra of T-450, TP0.5-450, TP1.0-450, and TP1.50-450. **b** Graphic displays the region from 1200 to 950 cm^{-1} showing the chemical environment of the P in the TiO_2

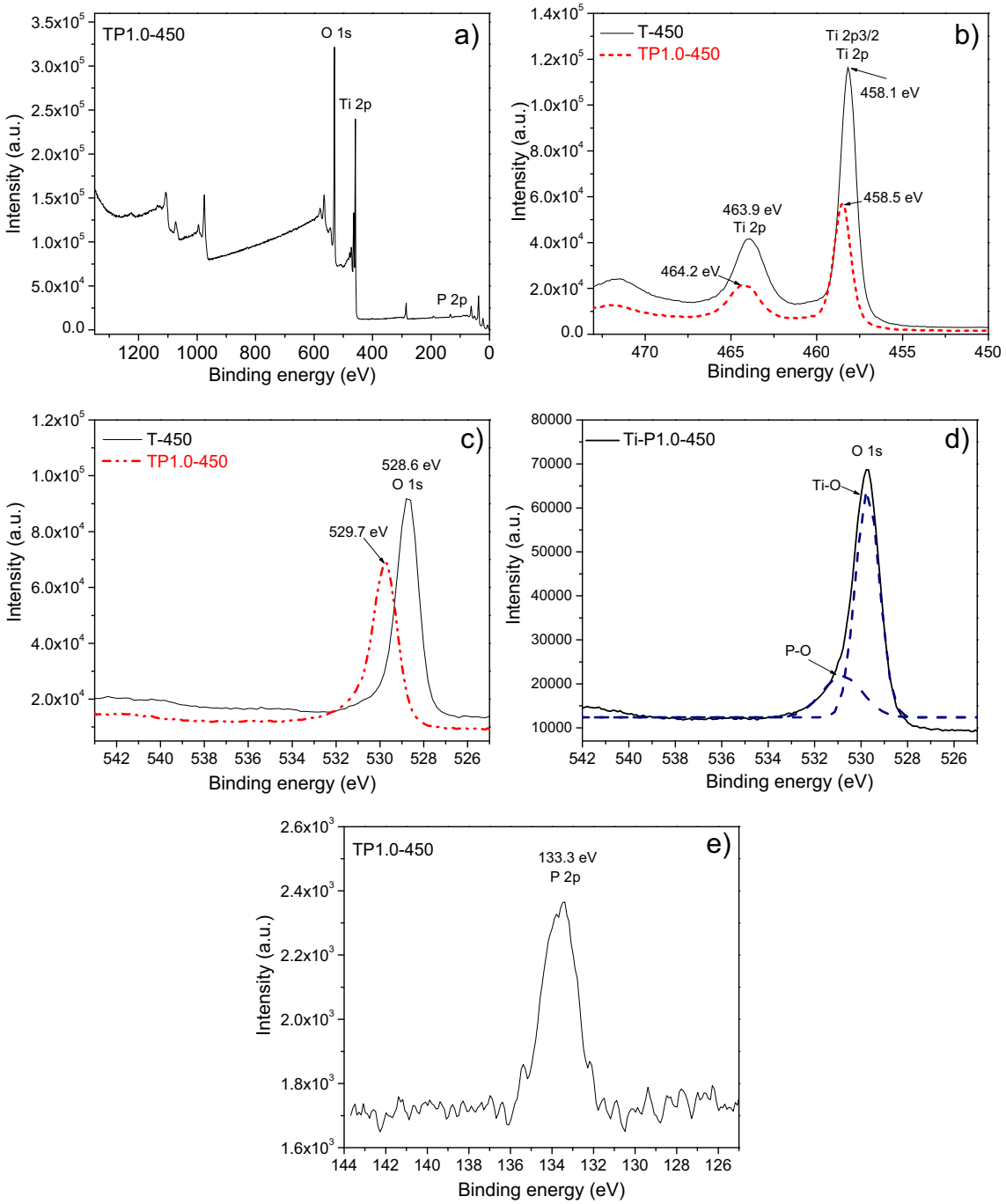

Fig. 5 XPS spectra. **a** TP1.0-450. **b** Ti 2p for TP-1.0 and as a reference T. **c** O 1s for TP1.0-450 and as a reference. **d** O 1s TP1.0-450. **e** P 2p for TP1.0-450

Photocatalytic activity evaluation

In the current study, photocatalytic activity of T and TP materials was carried out on a batch reactor using 10 mg/L SMTZ solution (as a model contaminant) with fixed catalyst loading of 1 g/L that were key features to make future comparisons more precise. Pollution concentration level was similar to that previously reported on SMTZ degradation by photocatalytic process (Babić et al. 2015; Tzeng et al. 2016). The amount of catalyst concentration was based on previous reports on a batch reactor. The catalyst loading affects both the number of active sites on photocatalysts and the penetration of UV light through the suspension. The optimum value of catalyst loading has been reported to be 1 g/L for photocatalytic degradation of several organic pollutants such as MCPA, ever direct blue and SMTZ in batch reactors (Mendiola et al. 2017; Akpan and Hameed 2009; Guo et al. 2013). The solution pH for photocatalytic experiments was adjusted to pH 8. In a preliminary experiment, the effect of solution pH on the photocatalytic performance of TP1.0-450 material was

evaluated. Differences in degradation percentage (at 180 min) and rate constant following pseudo-first-order kinetic model were observed when SMTZ solution was adjusted at pH 3.0 (67.2% and $k_{app} = 9.1 \times 10^{-3}$ min^{-1}), 5.5 (85.0% and $k_{app} = 14.7 \times 10^{-3}$ min^{-1}), and 8.0 (92.1% and $k_{app} = 22.4 \times 10^{-3}$ min^{-1}). Those results indicated that better photocatalytic performance of TP1.0-450 was achieved at pH 8. SMTZ has two p*K*a values (2.79 and 7.49); thus, SMTZ is not in fully deprotonated at pH value of 8 (79% the portion of SMTZ is anionic form) (Lertpaitoonpan et al. 2009). On the other hand, the TP catalyst could be negatively charged due to doping with P decrease the point of zero zeta potential of TiO_2 (Devi and Kavitha 2013). It was reported by Yu et al. (2003) that there was a decrease of isoelectric point in terms of pH from 5.8 (TiO_2) to 5.4 (TiO_2-P) when P was incorporated in 0.7 wt%. It has also been described that the presence of the phosphate anion, bounded at the surface of TiO_2 in the P-doped TIO_2 materials as observed in the prepared catalysts (see Fig. 4), disseminates the accumulation of negative charges on the surface of the catalyst that promotes the separation of electrons/holes increasing the photocatalytic activity (Zhao et al. 2008). Moreover, highest concentration of ^{-}OH was present on SMTZ solution adjusted to pH 8 (Guo et al. 2013); thus, the presence of these reactive species could enhance the electrostatic attraction of neutral SMTZ molecule and the $^{\bullet}OH$, who is the responsible of the attack at SMTZ molecule (Yap et al. 2012).

The effect of P doping (Fig. 6a) on the photocatalytic degradation of SMTZ was evaluated at different percentages of P (0.5, 1.0, and 1.5%). The degradation efficiency of TP1.0-450 was found to be better as compared to the other percentage of P (wt%) amount in TP samples. The degradation percentages at 300 min reaction were 76.4, 90.5, 100.0, and 87.7% for T-450, TP0.5-450, TP1.0-450, and TP1.5-450, respectively. Those results were in agreement with previous studies. For instance, Yu et al. (2003) indicated that P-doped TiO_2 with P addition in amount of 1.0 wt% showed better photocatalytic activity. The photocatalytic degradation of SMTZ at liquid–solid interface has been described by the Langmuir–Hinshelwood's (Eq. 2) kinetic model (Kaniou et al. 2005; Guo et al. 2013).

$$r = -\frac{dC}{dt} = k_{LH}\frac{K_L C_0}{1 + K_L C_0} \tag{2}$$

where

k_{LH} Langmuir–Hinshelwood reaction rate constant
K_L Reactant adsorption constant
C_0 Initial concentration of SMTZ

When the SMTZ concentration is low, it is considered a pseudo-first-order reaction, where k_{app} is velocity constant, C is concentration of SMTZ at determinate time, and C_0 is the initial concentration (Eq. 3).

$$\ln\left(\frac{C}{C_0}\right) = -k_{app}t \tag{3}$$

The degradation reaction rate can be expressed as pseudo-first-order model with correlation coefficients (R^2) higher than 0.9853, indicating reasonably good fit of the experimental data to the kinetic model. The degradation rate constants of SMTZ were 12.3×10^{-3}, 16.84×10^{-3}, and 11.6×10^{-3} (min^{-1}) for TP0.5-450, TP1.0-450, and TP1.5-450, respectively, while T-450 and DP25 showed 5.2×10^{-3} and 2.1×10^{-3} (min^{-1}) degradation rate. The effect of P-doping content (0.1–2.0 wt%) on the

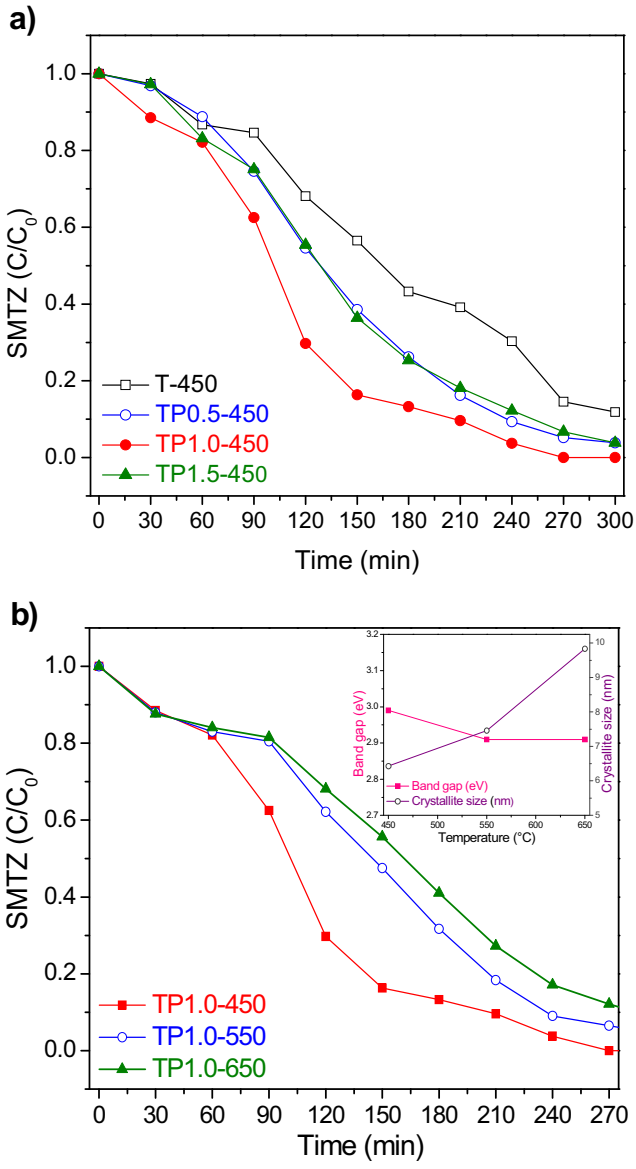

Fig. 6 Degradation of SMTZ (10 mg/L) at pH 8 under visible light **a** with different percentages of P and **b** different temperatures of calcination and indexed graphic crystallite size and Eg values of TP1.0 calcined at different temperatures

photocatalytic performance of P-doped TiO_2 samples has been evaluated by some authors (Yu et al. 2003; Wang and Zhou 2011; Gopal et al. 2012; Iwase et al. 2013b; Mohamed and Aazam 2013). The optimal doping amount found in this study was in agreement with previous published studies where P-doping content between 0.7 and 1.94 wt% (Yu et al. 2003; Gopal et al. 2012; Mohamed and Aazam 2013) could inhibit the recombination between photogenerated electron and holes (Shi et al. 2006; Li et al. 2009; Xia et al. 2014). Nevertheless, when the amount was higher than the optimal value, the phosphorous become a recombination center of photogenerated electron and holes (Li et al. 2009). Different authors (Li et al. 2009; Zhang et al. 2009) proved that incorporation of phosphorus is an effective method in stabilizing the anatase phase at high temperature. The result was confirmed by XRD technique. However, the increase in calcination temperature affected photocatalytic activity of the tested materials. As shown in Fig. 6b, the increment of the calcination temperature in the P-doped TiO_2 materials decreased the degradation percentage of SMTZ at 300 min in the order 450 > 550 > 650 °C (100.0, 90.1, and 86.9%, respectively). This result can be attributed to the increase in the crystallite size when raised the calcination temperature, although the Eg values slightly decreased in approximately 0.08 eV for the materials with high calcination temperature (inset graphic in Fig. 6b). The same effect of temperature was observed by Chen et al. (2011), and they, besides the increment of crystallite size, attributed the decrease of degradation process to phosphate group who acts like a barrier on the surface inhibiting the crystal coalescence and retaining the anatase phase. Thus, TP1.0-450 sample showed better performance on degradation of SMTZ. Control experiments were carried out (see Fig. 7a) to evaluate the adsorption capacity of the catalyst TP1.0-450 in the absence of light and the stability of the contaminant during the photolysis process. Negligible degradation of SMTZ was carried out by these two processes. In the same graphic, the results of the photodegradation of SMTZ with TP materials and for comparative purpose with T-450 and DP25 are shown. As can be seen, the highest photocatalytic performance on degradation of SMTZ was carried out with TP1.0-450 with a degradation percentage of 100%, followed by the T-450 catalyst with 76.4% and DP25 with 67.2%. The poor activity for commercial and undoped TiO_2 could be attributed to their large crystallite size and smaller specific surface area (Kaniou et al. 2005). Also, it is well known that TiO_2 had a low activity under visible light due to its large band gap.

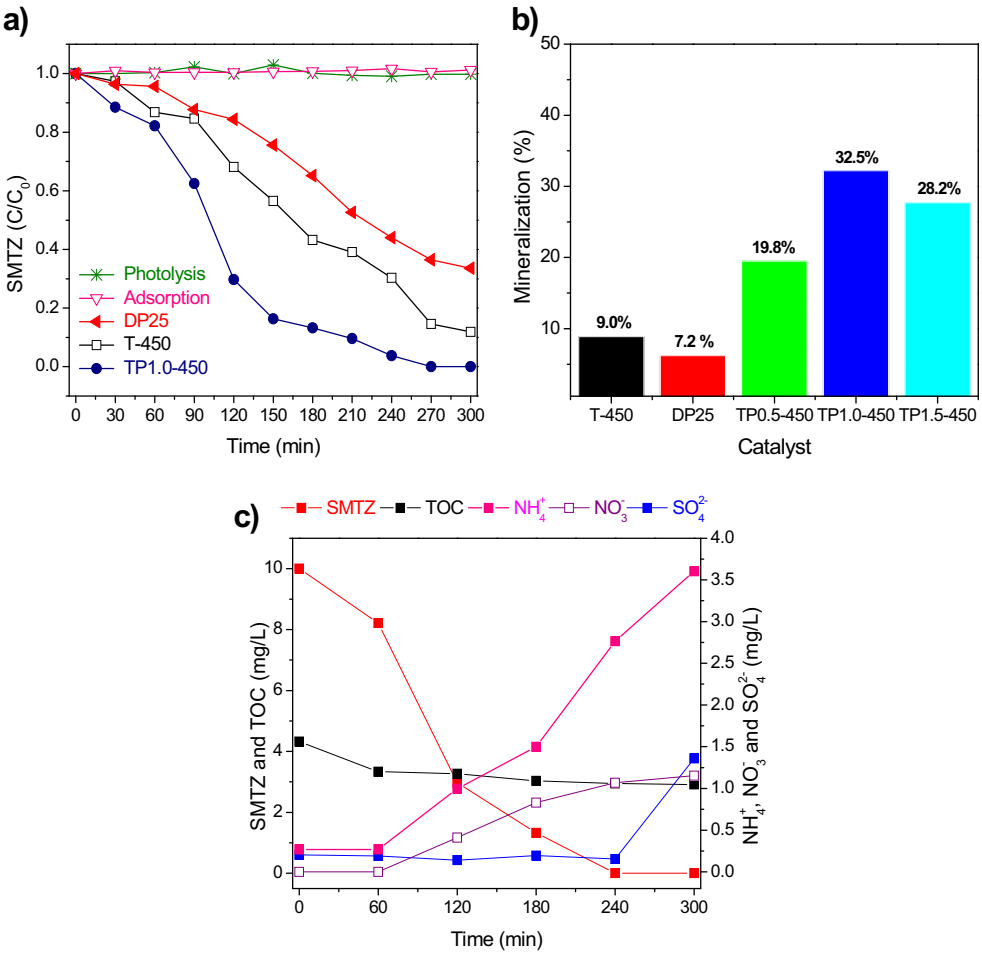

Fig. 7 Degradation of SMTZ (10 mg/L) at pH 8 with **a** adsorption with TP1.0-450, photolysis, and photocatalytic activity with DP25, T-450, and TP1.0-450 and **b** mineralization with T-450, TP0.5-450, TP1.0-450, TP1.50-450, and DP25 at 300 min. **c** Evaluation of degradation, mineralization, and evolution of cation and anions with TP1.0-450

Comparing with P-doped materials, Ti-450 had low amount of surface hydroxyl group, reported as a responsible of the photoactivity (Zhao et al. 2008). Other authors like Chen et al. (2011); Kuo et al. (2015) attributed to the hydroxyl group present in TP materials (confirmed by FTIR spectra; Fig. 4) the enhanced photocatalytic activity.

TOC removal efficiency was evaluated for the undoped and doped materials calcinated at 450 °C. As shown in Fig. 7b, the highest value was obtained by TP1.0-450 (32.5%) followed by TP1.5-450 > TP0.5-450 > T-450 > DP25, which showed the same trend as degradation process (Fig. 7a). The low mineralization percentage could be attributed to the stability and recalcitrant nature of SMTZ (Liu and Wang 2013), and their open-ring by-products 4,6-dimethylpyrimidine and aniline were generated during SMTZ oxidation (Tzeng et al. 2016). These results were in agreement with previous photocatalytic studies that showed lower mineralization percentage of SMTZ (15–23%) under UV radiation with TiO_2 (Babić et al. 2015; Tzeng et al. 2016).

The evolution of ions (NH_4^+, NO_3^-, and SO_4^{2-}) during the degradation and mineralization of SMTZ is shown in Fig. 7c. The inorganic nitrogen species NH_4^+ and NO_3^- ions were identified during SMTZ degradation. The predominant species was NH_4^+ (1.24 mg/L) followed by NO_3^- (0.60 mg/L) at 300 min of reaction. The nitrogen mass balance during the photocatalytic degradation of SMTZ indicated that only 43% was released. The SO_4^{2-} ion was also identified during the oxidation of SMTZ in concentration of 0.35 mg/L at 300 min reaction. The mass balance of sulfur during this reaction indicated that only 10% was released. With these results, a possible degradation mechanism could be inferred. Accordingly, with the literature at solution pH higher than pKa_2 of SMTZ (7.45), the –NH sulfonamide group is deprotonated and this could allow the photocatalytic oxidation mainly through hydroxyl radical-mediated pathway (Fan et al. 2015), producing 4,6-dimethylpyrimidin-2-amine and sulfanilic acid intermediates (Liu and Wang 2013). The extrusion of SO_4^{2-} could generate other intermediates as *N*-(4,6-dimethyl- pyrimidin-2yl)benzene-1,4-diamine, benzene-1,4-diamine, 4-aminophenol, and 4,6-dimethylpyrimidin-2-ol described during the photocatalytic degradation of SMTZ under simulated solar radiation using Bi_2MoO_6 material (Guo et al. 2013).

Conclusions

The phosphorus-doped TiO_2 was successfully synthesized through the microwave-assisted sol-gel method with calcination temperatures ranging from 450 to 650 °C. The incorporation of phosphorus has proved to be an effective method in stabilizing the anatase phase at high temperature. The highest degradation percentage (100%) and mineralization efficiency (32.5%) were reached with a P doping content of 1.0 (wt%) on TiO_2 sample calcined at 450 °C (TP1.0-450). The TP1.0-450 material exhibited significantly higher photocatalytic activity than undoped T-450 and DP25 on SMTZ degradation. This enhanced activity was attributable to a combination of its higher surface area with mesoporous ordering and smaller crystallite size, particle size, and band gap values. Moreover, the TP material showed more hydroxyl groups on its surface as demonstrated by FTIR. Thus, the P doping in TiO_2 as superficial phosphate ($PO4^{3-}$) and incorporation as P^{5+} oxidation state substituting the lattice Ti^{4+} to form Ti-O-P reduced the recombination of the e^-/h^+ pairs of the TP semiconductor, enhancing its photoactivity. Evolution of ammonium, nitrate, and sulfate during SMTZ degradation using TP1.0-450 material indicated that the oxidation process involves the extrusion of these ions from SMTZ molecule. However, the complete mineralization of SMZT during photocatalytic degradation with TP1.0-450 was not achieved with TP1.0-450 under visible radiation due to the recalcitrant nature of this nitrogen-heterocyclic compound.

Acknowledgements Mendiola-Alvarez thanks the CONACYT for her doctorate scholarship.

Funding information The authors gratefully acknowledge financial support from PAICYT UANL and Facultad de Ciencias Químicas, UANL.

References

Akpan U, Hameed B (2009) Parameters affecting the photocatalytic degradation of dyes using TiO_2-based photocatalysts: a review. J Hazard Mater 170:520–529. https://doi.org/10.1016/j.jhazmat.2009.05.039

Ansari S, Cho M (2016) Highly visible light responsive, narrow band gap TiO_2 nanoparticles modified by elemental red phosphorus for photocatalysis and photoelectrochemical applications. Sci Rep 6: 1–10. https://doi.org/10.1038/srep25405

Babić S, Zrnčić M, Ljubas D (2015) Photolytic and thin TiO_2 film assisted photocatalytic degradation of sulfamethazine in aqueous solution. Environ Sci Pollut Res 22:11372–11386. https://doi.org/10.1007/s11356-015-4338-5

Bahadur S, Bera S, Lee D (2013) Design of visible-light photocatalysts by coupling of narrow bandgap semiconductors and TiO_2: effect of their relative energy band positions on the photocatalytic efficiency. Catal Sci Technol 3:1822–1830. https://doi.org/10.1039/c3cy00004d

Batt A, Snow D, Aga D (2006) Occurrence of sulfonamide antimicrobials in private water wells in Washington County, Idaho, USA. Chemosphere 64:1963–1971. https://doi.org/10.1016/j.chemosphere.2006.01.029

Ben W, Qiang Z, Yin X (2014) Adsorption behavior of sulfamethazine in an activated sludge process treating swine wastewater. J Environ Sci 26:1623–1629. https://doi.org/10.1016/j.jes.2014.06.002

Cervantes M (2012) Diseño y síntesis de materiales a "medida" mediante el método sol-gel, UNED

Chen J, Shunchen Q, Yuexiang Z, Youchang X (2011) Phosphorous-modified TiO_2 with excellent thermal stability and its application to the degradation of pollutants in water. Chin J Catal 32:1173–1179. https://doi.org/10.1016/S1872-2067(10)60229-X

Devi L, Kavitha R (2013) A review on non metal ion doped titania for the photocatalytic degradation of organic pollutants under UV/solar

light: role of photogenerated charge carrier dynamics in enhancing the activity. Appl Catal B Environ 140–141:559–587. https://doi.org/10.1016/j.apcatb.2013.04.035

Elghniji K, Soro J, Rossignol S, Ksibi M (2012) A simple route for the preparation of P-modified TiO_2: effect of phosphorus on thermal stability and photocatalytic activity. J Taiwan Inst Chem Eng 43:132–139. https://doi.org/10.1016/j.jtice.2011.06.011

Ermokhina N, Nevinskiy V, Manorik P (2013) Synthesis and characterization of thermally stable large-pore mesoporous nanocrystalline anatase. J Solid State Chem 200:90–98. https://doi.org/10.1016/j.jssc.2012.12.034

Fan Y, Ji Y, Kong D (2015) Kinetic and mechanistic investigations of the degradation of sulfamethazine in heat-activated persulfate oxidation process. J Hazard Mater 300:39–47. https://doi.org/10.1016/j.jhazmat.2015.06.058

García M, Villagrasa M, Díaz M, Barceló D (2010) LC-QqLIT MS analysis of nine sulfonamides and one of their acetylated metabolites in the Llobregat River basin. Quantitative determination and qualitative evaluation by IDA experiments. Anal Bioanal Chem 397:1325–1334. https://doi.org/10.1007/s00216-010-3630-y

Gopal N, Lo H, Ke T (2012) Visible light active phosphorus-doped TiO_2 nanoparticles: an EPR evidence for the enhanced charge separation. J Phys Chem C 116:16191–16197. https://doi.org/10.1021/jp212346f

Guo S, Wang F, Sun J (2010) Marked enhancement of photocatalytic activity of P-doped TiO_2 with hydrothermal method. Adv Mater Res 113–116:2150–2215. https://doi.org/10.4028/www.scientific.net/AMR.113-116.2150

Guo C, Xu J, Wang S (2013) Photodegradation of sulfamethazine in an aqueous solution by a bismuth molybdate photocatalyst. Catal Sci Technol 3:160. https://doi.org/10.1039/c3cy20811g

Hsuan-Fu Y (2007) Photocatalytic abilities of gel-derived P-doped TiO_2. J Phys Chem Solids 68:600–607. https://doi.org/10.1016/j.jpcs.2007.01.050

Iwase M, Yamada K, Kurisaki T (2013a) A study on the active sites for visible-light photocatalytic activity of phosphorus-doped titanium (IV) oxide particles prepared using a phosphide compound. Appl Catal B Environ 141:327–332

Iwase M, Yamada K, Kurisaki T (2013b) Visible-light photocatalysis with phosphorus-doped titanium (IV) oxide particles prepared using a phosphide compound. Appl Catal B Environ 132–133:39–34. https://doi.org/10.1016/j.apcatb.2012.11.014

Kaniou S, Pitarakis K, Barlagianni I, Poulios I (2005) Photocatalytic oxidation of sulfamethazine. Chemosphere 60:372–380. https://doi.org/10.1016/j.chemosphere.2004.11.069

Kesong Y, Ying D, Baibiao H (2007) Understanding photocatalytic activity of S- and P-doped TiO_2 under visible light from first-principles. J Phys Chem C 51:18985–18994

Körösi L, Papp S, Bertóti I, Dékány I (2007) Surface and bulk composition, structure, and photocatalytic activity of phosphate-modified TiO_2. Chem Mater 19:4811–4819. https://doi.org/10.1021/cm070692r

Kuo C, Wu C, Wu J, Chen Y (2015) Synthesis and characterization of a phosphorus-doped TiO_2 immobilized bed for the photodegradation of bisphenol A under UV and sunlight irradiation. React Kinet Mech Catal 114:753–766. https://doi.org/10.1007/s11144-014-0783-2

Lertpaitoonpan W, Ong S, Moorman T (2009) Effect of organic carbon and pH on soil sorption of sulfamethazine. Chemosphere 76:558–564. https://doi.org/10.1016/j.chemosphere.2009.02.066

Li F, Jiang Y, Xia M (2009) Effect of the P/Ti ratio on the visible-light photocatalytic activity of P-doped TiO_2. J Phys Chem 113:18134–18141

Lin L, Zheng R, Xie J (2007) Synthesis and characterization of phosphor and nitrogen co-doped titania. Appl Catal B Environ 76:196–202. https://doi.org/10.1016/j.apcatb.2007.05.023

Liu Y, Wang J (2013) Degradation of sulfamethazine by gamma irradiation in the presence of hydrogen peroxide. J Hazard Mater 250–251:99–105. https://doi.org/10.1016/j.jhazmat.2013.01.050

Lv Y, Yu L, Huang H (2009) Preparation, characterization of P-doped TiO_2 nanoparticles and their excellent photocatalystic properties under the solar light irradiation. J Alloys Compd 488:314–319. https://doi.org/10.1016/j.jallcom.2009.08.116

Ma L, Jia I, Guo X, Xiang L (2014) Current status and perspective of rare earth catalytic materials and catalysis. Chin J Catal 35:108–119. https://doi.org/10.1016/S1872

Martinez J (2009) Environmental pollution by antibiotics and by antibiotic resistance determinants. Environ Pollut 157:2893–2902. https://doi.org/10.1016/j.envpol.2009.05.051

Mendiola S, Guzmán J, Turnes G, Maya A, Hernández A, Hinojosa L (2017) UV and visible activation of Cr(III)-doped TiO_2 catalyst prepared by a microwave-assisted sol–gel method during MCPA degradation. Environ Sci Pollut Res 24:12673–12682. https://doi.org/10.1007/s11356-016-8034-x

Miranda N, Suárez S, Maldonado M (2014) Regeneration approaches for TiO_2 immobilized photocatalyst used in the elimination of emerging contaminants in water. Catal Today 230:27–34. https://doi.org/10.1016/j.cattod.2013.12.048

Mohamed R, Aazam E (2013) Synthesis and characterization of P-doped TiO_2 thin-films for photocatalytic degradation of butyl benzyl phthalate under visible-light irradiation. Chin J Catal 34:1267–1273. https://doi.org/10.1016/S1872-2067(12)60572-5

Niu J, Lu P, Kang M (2014) P-doped TiO_2 with superior visible-light activity prepared by rapid microwave hydrothermal method. Appl Surf Sci 319:99–106. https://doi.org/10.1016/j.apsusc.2014.07.048

Shi Q, Yang D, Jiang Z, Li J (2006) Visible-light photocatalytic regeneration of NADH using P-doped TiO_2 nanoparticles. J Mol Catal B Enzym 43:44–48. https://doi.org/10.1016/j.molcatb.2006.06.005

Sotelo C, Noor N, Kafizas A (2015) Multifunctional P-doped TiO_2 films: a new approach to self-cleaning, transparent conducting oxide materials. Chem Mater 27:3234–3242. https://doi.org/10.1021/cm504734a

Tongon W, Chawengkijwanich C, Chiarakorn S (2014) Visible light responsive Ag/TiO_2/MCM-41 nanocomposite films synthesized by a microwave assisted sol-gel technique. Superlattice Microst 69:108–121. https://doi.org/10.1016/j.spmi.2014.02.003

Tzeng T, Wang S, Chen C (2016) Photolysis and photocatalytic decomposition of sulfamethazine antibiotics in an aqueous solution with TiO_2. RSC Adv 6:69301–69310. https://doi.org/10.1039/C6RA13435A

Wang S, Zhou S (2011) Photodegradation of methyl orange by photocatalyst of CNTs/P-TiO_2 under UV and visible-light irradiation. J Hazard Mater 185:77–85. https://doi.org/10.1016/j.jhazmat.2010.08.125

Xia Y, Jiang Y, Li F (2014) Effect of calcined atmosphere on the photocatalytic activity of P-doped TiO_2. Appl Surf Sci 289:306–315. https://doi.org/10.1016/j.apsusc.2013.10.157

Yap P, Cheah Y, Srinivasan M, Lim T (2012) Bimodal N-doped P25-TiO_2/AC composite: preparation, characterization, physical stability, and synergistic adsorptive-solar photocatalytic removal of sulfamethazine. Appl Catal A Gen 427–428:125–136. https://doi.org/10.1016/j.apcata.2012.03.042

Yu J, Zhang L, Zheng Z, Zhao J (2003) Synthesis and characterization of phosphated mesoporous titanium dioxide with high photocatalytic activity. Chem Mater 15:2280–2286. https://doi.org/10.1021/cm0340781

Yu J, Xiang Q, Zhou M (2009) Preparation, characterization and visible-light-driven photocatalytic activity of Fe-doped titania nanorods and first-principles study for electronic structures. Appl Catal B Environ 90:595–602. https://doi.org/10.1016/j.apcatb.2009.04.021

Zhang Y, Fu W, Yang H (2009) Synthesis and characterization of P-doped TiO_2 nanotubes. 518:99–103. https://doi.org/10.1016/j.tsf.2009.06.051

Zhao D, Chen C, Wang Y (2008) Surface modification of TiO_2 by phosphate: effect on photocatalytic activity and mechanism implication. J Phys Chem C 112:5993–6001. https://doi.org/10.1021/jp712049c

Zhu Y, Zheng R, Lin L (2008) State of phosphor and its influence on the physicochemical and photocatalytic properties of P-doped titania. J Phys Chem C 112:15502–15509